

The INDRA-FAZIA setup:
an overview of the most recent results
on isospin transport phenomena

Caterina Ciampi
GANIL

for the INDRA-FAZIA collaboration

Colloque GANIL 2023
25-29 September 2023

Isospin transport phenomena

Nuclear symmetry energy at work in heavy ion reactions

Heavy ion collisions at intermediate energies → collect information on the

Isospin transport phenomena: projectile-target nucleon exchange processes

- governed by the *symmetry energy* term of the **Nuclear Equation of State**: energy per nucleon as a function of *density* $\rho = \rho_n + \rho_p$ and *isospin asymmetry*

$\delta = \frac{\rho_n - \rho_p}{\rho_n + \rho_p}$. By defining $x = \left(\frac{\rho - \rho_0}{3\rho_0}\right)$:

$$\frac{E}{A}(\rho, \delta) = \frac{E}{A}(\rho) + \frac{E_{sym}}{A}(\rho)\delta^2 \quad \text{where} \quad \frac{E_{sym}}{A}(\rho) = E_{sym} + L_{sym}x + \frac{1}{2}K_{sym}x^2 + \dots$$

Isospin transport phenomena

Nuclear symmetry energy at work in heavy ion reactions

Heavy ion collisions at intermediate energies → collect information on the

Isospin transport phenomena: projectile-target nucleon exchange processes

- governed by the *symmetry energy* term of the **Nuclear Equation of State**: energy per nucleon as a function of *density* $\rho = \rho_n + \rho_p$ and *isospin asymmetry*

$\delta = \frac{\rho_n - \rho_p}{\rho_n + \rho_p}$. By defining $x = \left(\frac{\rho - \rho_0}{3\rho_0}\right)$:

$$\frac{E}{A}(\rho, \delta) = \frac{E}{A}(\rho) + \frac{E_{sym}}{A}(\rho)\delta^2 \quad \text{where} \quad \frac{E_{sym}}{A}(\rho) = E_{sym} + L_{sym}x + \frac{1}{2}K_{sym}x^2 + \dots$$

- The **isospin transport phenomena** can be expressed as:

$$\mathbf{j}_n - \mathbf{j}_p \propto \frac{E_{sym}}{A}(\rho)\nabla\delta + \delta\frac{\partial\frac{E_{sym}}{A}(\rho)}{\partial\rho}\nabla\rho$$

Isospin transport phenomena

Nuclear symmetry energy at work in heavy ion reactions

Heavy ion collisions at intermediate energies → collect information on the

Isospin transport phenomena: projectile-target nucleon exchange processes

- governed by the *symmetry energy* term of the **Nuclear Equation of State**: energy per nucleon as a function of *density* $\rho = \rho_n + \rho_p$ and *isospin asymmetry*

$\delta = \frac{\rho_n - \rho_p}{\rho_n + \rho_p}$. By defining $x = \left(\frac{\rho - \rho_0}{3\rho_0}\right)$:

$$\frac{E}{A}(\rho, \delta) = \frac{E}{A}(\rho) + \frac{E_{sym}}{A}(\rho)\delta^2 \quad \text{where} \quad \frac{E_{sym}}{A}(\rho) = E_{sym} + L_{sym}x + \frac{1}{2}K_{sym}x^2 + \dots$$

- The **isospin transport phenomena** can be expressed as:

$$\mathbf{j}_n - \mathbf{j}_p \propto \frac{E_{sym}}{A}(\rho)\nabla\delta + \delta\frac{\partial\frac{E_{sym}}{A}(\rho)}{\partial\rho}\nabla\rho$$

- Isospin diffusion:** driven by an isospin gradient in the system (e.g. asymmetric systems), leading to isospin equilibration.

Sensitive to $E_{sym}(\rho)/A$

Isospin transport phenomena

Nuclear symmetry energy at work in heavy ion reactions

Heavy ion collisions at intermediate energies → collect information on the

Isospin transport phenomena: projectile-target nucleon exchange processes

- governed by the *symmetry energy* term of the **Nuclear Equation of State**: energy per nucleon as a function of *density* $\rho = \rho_n + \rho_p$ and *isospin asymmetry*

$$\delta = \frac{\rho_n - \rho_p}{\rho_n + \rho_p}. \text{ By defining } x = \left(\frac{\rho - \rho_0}{3\rho_0} \right):$$

$$\frac{E}{A}(\rho, \delta) = \frac{E}{A}(\rho) + \frac{E_{sym}}{A}(\rho)\delta^2 \quad \text{where} \quad \frac{E_{sym}}{A}(\rho) = E_{sym} + L_{sym}x + \frac{1}{2}K_{sym}x^2 + \dots$$

- The **isospin transport phenomena** can be expressed as:

$$\mathbf{j}_n - \mathbf{j}_p \propto \frac{E_{sym}}{A}(\rho)\nabla\delta + \delta \frac{\partial \frac{E_{sym}}{A}(\rho)}{\partial \rho} \nabla\rho$$

- Isospin diffusion:** driven by an isospin gradient in the system (e.g. asymmetric systems), leading to isospin equilibration.
Sensitive to $E_{sym}(\rho)/A$
- Isospin drift** (or *isospin migration*): driven by density gradient (e.g. neck $\rho \lesssim \rho_0$). Can be isolated by choosing a symmetric system.

Sensitive to $\frac{\partial E_{sym}(\rho)/A}{\partial \rho}$

Isospin transport phenomena

Nuclear symmetry energy at work in heavy ion reactions

Heavy ion collisions at intermediate energies → collect information on the

Isospin transport phenomena: projectile-target nucleon exchange processes

- governed by the *symmetry energy* term of the **Nuclear Equation of State**: energy per nucleon as a function of *density* $\rho = \rho_n + \rho_p$ and *isospin asymmetry*

$$\delta = \frac{\rho_n - \rho_p}{\rho_n + \rho_p}. \text{ By defining } x = \left(\frac{\rho - \rho_0}{3\rho_0} \right):$$

$$\frac{E}{A}(\rho, \delta) = \frac{E}{A}(\rho) + \frac{E_{sym}}{A}(\rho)\delta^2 \quad \text{where} \quad \frac{E_{sym}}{A}(\rho) = E_{sym} + L_{sym}x + \frac{1}{2}K_{sym}x^2 + \dots$$

- The **isospin transport phenomena** can be expressed as:

$$\mathbf{j}_n - \mathbf{j}_p \propto \frac{E_{sym}}{A}(\rho)\nabla\delta + \delta \frac{\partial \frac{E_{sym}}{A}(\rho)}{\partial \rho} \nabla\rho$$

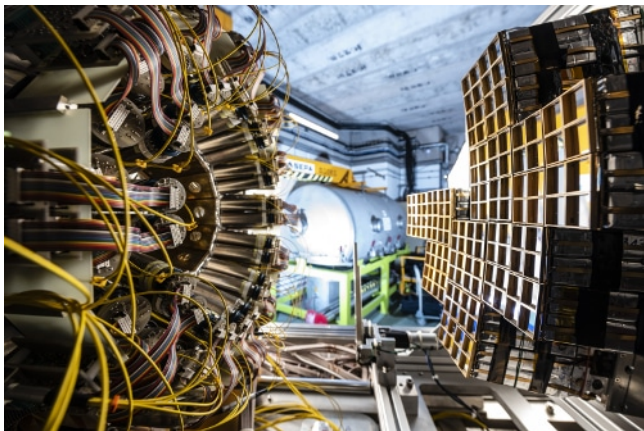
- Isospin diffusion:** driven by an isospin gradient in the system (e.g. asymmetric systems), leading to isospin equilibration. Sensitive to $E_{sym}(\rho)/A$ → **QP-QT isospin equilibration**
- Isospin drift** (or *isospin migration*): driven by density gradient (e.g. neck $\rho \lesssim \rho_0$). Can be isolated by choosing a symmetric system.

Sensitive to $\frac{\partial E_{sym}(\rho)/A}{\partial \rho}$ → **neutron enrichment of the neck region**

INDRA-FAZIA

The coupling of the two setups

INDRA and FAZIA: multi-detector apparatuses, designed for the detection of nuclear fragments produced heavy ion collisions at Fermi energies. Their characteristics are in some respects complementary.



During the first months of 2019 the coupling between INDRA and FAZIA was completed in GANIL.

INDRA-FAZIA

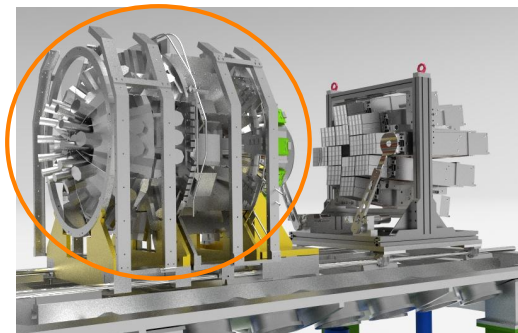
The coupling of the two setups



- The most forward polar angles ($1.4^\circ < \theta < 12.6^\circ$) have been covered with 12 FAZIA blocks in a wall configuration at 1 m from the target. The first five rings of INDRA have been removed.
→ *isotopic identification of QP-like fragments*

INDRA-FAZIA

The coupling of the two setups



- The most forward polar angles ($1.4^\circ < \theta < 12.6^\circ$) have been covered with 12 FAZIA blocks in a wall configuration at 1 m from the target. The first five rings of INDRA have been removed.
→ *isotopic identification of QP-like fragments*
- The remaining part of INDRA (rings 6-17) covers the polar angles between 14° and 176° ($\sim 80\%$ of the 4π solid angle).
→ *global variables for the estimation of the reaction centrality*

INDRA-FAZIA

The first experiments at GANIL

After the INDRA-FAZIA coupling, two experiments have been carried out at GANIL:

- E789 (2019): $^{58,64}\text{Ni}+^{58,64}\text{Ni}$ at 32, 52 MeV/nucl.
C. Ciampi et al., Phys. Rev. C 106, 024603 (2022),
C. Ciampi et al., arXiv:2308.15077 [nucl-ex] (2023)
- E818 (2022): $^{58}\text{Ni},^{36}\text{Ar}+^{58}\text{Ni}$ at 74 MeV/nucl.
data reduction is now finished, analysis in progress
→ see talk by Lucia Baldesi



INDRA-FAZIA

The first experiments at GANIL

After the INDRA-FAZIA coupling, two experiments have been carried out at GANIL:

- **E789 (2019):** $^{58,64}\text{Ni}+^{58,64}\text{Ni}$ at 32, 52 MeV/nucl.
C. Ciampi et al., Phys. Rev. C 106, 024603 (2022),
C. Ciampi et al., arXiv:2308.15077 [nucl-ex] (2023)
- **E818 (2022):** $^{58}\text{Ni}, ^{36}\text{Ar}+^{58}\text{Ni}$ at 74 MeV/nucl.
data reduction is now finished, analysis in progress
→ see talk by Lucia Baldesi



The isospin diffusion mechanism was the main topic of the **E789 experiment**:

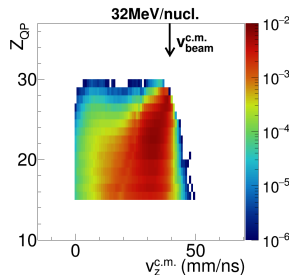
- All of the four possible combinations of the two reaction partners ^{58}Ni and ^{64}Ni have been studied
⇒ compare the products of the two asymmetric reactions with those of both the neutron rich and neutron deficient symmetric systems
- Two different incident beam energies 32 MeV/nucl and 52 MeV/nucl.
⇒ different timescale of the interaction process and different inspected nuclear density range

Binary output channel

Study of the QP evaporation channel

Main goal: focus on the binary exit channel for semiperipheral and peripheral collisions

- selected as $M_{big} = 1$, with $Z_{big} \geq 15$ and $\theta_{big}^{CM} < 90^\circ$ ($v_z^{CM} > 0$) \rightarrow QP remnant

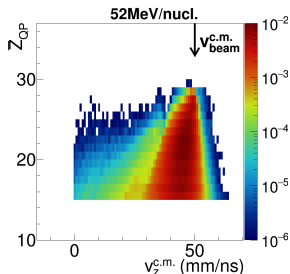


Binary output channel

Study of the QP evaporation channel

Main goal: focus on the binary exit channel for semiperipheral and peripheral collisions

- selected as $M_{\text{big}} = 1$, with $Z_{\text{big}} \geq 15$ and $\theta_{\text{big}}^{\text{CM}} < 90^\circ$ ($v_z^{\text{CM}} > 0$) \rightarrow QP remnant
- AMD+GEMINI++ simulations satisfactorily reproduce the main features for this QP evaporation channel



Binary output channel

Study of the QP evaporation channel

Main goal: focus on the binary exit channel for semiperipheral and peripheral collisions

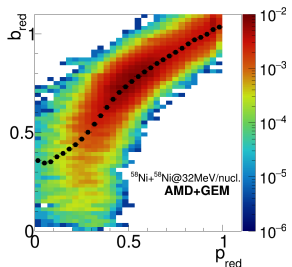
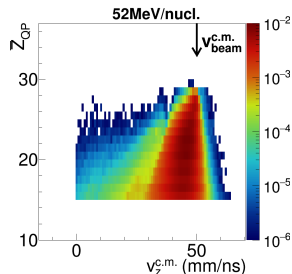
- selected as $\mathbf{M}_{\text{big}} = 1$, with $Z_{\text{big}} \geq 15$ and $\theta_{\text{big}}^{\text{CM}} < 90^\circ$ ($v_z^{\text{CM}} > 0$) \rightarrow QP remnant
- AMD+GEMINI++ simulations satisfactorily reproduce the main features for this **QP evaporation channel**

As reaction centrality estimator we select the

reduced momentum along the z-axis: $p_{\text{red}} = \frac{p_z^{\text{QP}}}{p_{\text{beam}}}$

Its correlation with $b_{\text{red}} = b/b_{\text{gr}}$ is:

- reliable for $p_{\text{red}} \gtrsim 0.3$



Binary output channel

Study of the QP evaporation channel

Main goal: focus on the binary exit channel for semiperipheral and peripheral collisions

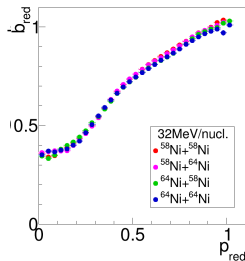
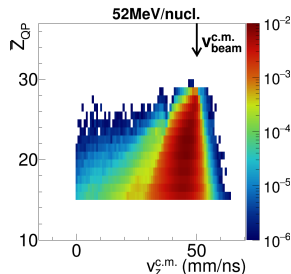
- selected as $\mathbf{M}_{\text{big}} = 1$, with $Z_{\text{big}} \geq 15$ and $\theta_{\text{big}}^{\text{CM}} < 90^\circ$ ($v_z^{\text{CM}} > 0$) \rightarrow QP remnant
- AMD+GEMINI++ simulations satisfactorily reproduce the main features for this **QP evaporation channel**

As reaction centrality estimator we select the

reduced momentum along the z-axis: $p_{\text{red}} = \frac{p_z^{\text{QP}}}{p_{\text{beam}}}$

Its correlation with $b_{\text{red}} = b/b_{\text{gr}}$ is:

- reliable for $p_{\text{red}} \gtrsim 0.3$
- the same for reactions at same energy



Binary output channel

Study of the QP evaporation channel

Main goal: focus on the binary exit channel for semiperipheral and peripheral collisions

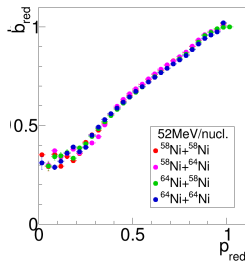
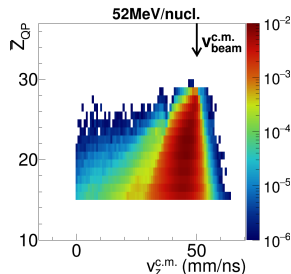
- selected as $\mathbf{M}_{\text{big}} = 1$, with $Z_{\text{big}} \geq 15$ and $\theta_{\text{big}}^{\text{CM}} < 90^\circ$ ($v_z^{\text{CM}} > 0$) \rightarrow QP remnant
- AMD+GEMINI++ simulations satisfactorily reproduce the main features for this **QP evaporation channel**

As reaction centrality estimator we select the

reduced momentum along the z-axis: $p_{\text{red}} = \frac{p_z^{\text{QP}}}{p_{\text{beam}}}$

Its correlation with $b_{\text{red}} = b/b_{\text{gr}}$ is:

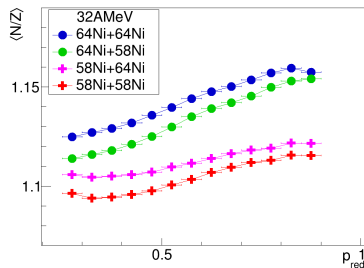
- reliable for $p_{\text{red}} \gtrsim 0.3$
- the same for reactions at same energy
- similar for same system at two energies



QP evaporation channel in Ni+Ni collisions

Isospin diffusion: $\langle N/Z \rangle$ of the QP remnant

Evolution of $\langle N/Z \rangle$ of the QP remnant with centrality \rightarrow **evidence of isospin diffusion**



QP evaporation channel in Ni+Ni collisions

Isospin diffusion: $\langle N/Z \rangle$ of the QP remnant

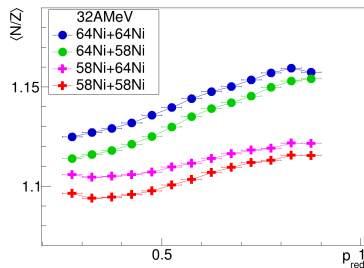
Evolution of $\langle N/Z \rangle$ of the QP remnant with centrality \rightarrow **evidence of isospin diffusion**

Isospin transport ratio: can highlight the effect, bypassing the effects acting similarly on the four systems (F. Rami et al., Phys. Rev. Lett. 84, 1120 (2000))

Given $A = {}^{64}\text{Ni}$, $B = {}^{58}\text{Ni}$:

$$R(X) = \frac{2X_i - X_{AA} - X_{BB}}{X_{AA} - X_{BB}}$$

where $i = AA, AB, BA, BB$ and X is an isospin sensitive observable (e.g. $\langle N/Z \rangle_{QP}$).



QP evaporation channel in Ni+Ni collisions

Isospin diffusion: $\langle N/Z \rangle$ of the QP remnant

Evolution of $\langle N/Z \rangle$ of the QP remnant with centrality \rightarrow **evidence of isospin diffusion**

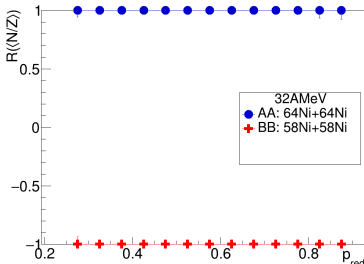
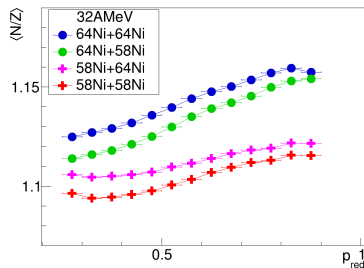
Isospin transport ratio: can highlight the effect, bypassing the effects acting similarly on the four systems (F. Rami et al., Phys. Rev. Lett. 84, 1120 (2000))

Given $A = {}^{64}\text{Ni}$, $B = {}^{58}\text{Ni}$:

$$R(X) = \frac{2X_i - X_{AA} - X_{BB}}{X_{AA} - X_{BB}}$$

$R(X) = \pm 1 \rightarrow$ non eq.

where $i = AA, AB, BA, BB$ and X is an isospin sensitive observable (e.g. $\langle N/Z \rangle_{QP}$).



QP evaporation channel in Ni+Ni collisions

Isospin diffusion: $\langle N/Z \rangle$ of the QP remnant

Evolution of $\langle N/Z \rangle$ of the QP remnant with centrality \rightarrow **evidence of isospin diffusion**

Isospin transport ratio: can highlight the effect, bypassing the effects acting similarly on the four systems (F. Rami et al., Phys. Rev. Lett. 84, 1120 (2000))

Given $A = {}^{64}\text{Ni}$, $B = {}^{58}\text{Ni}$:

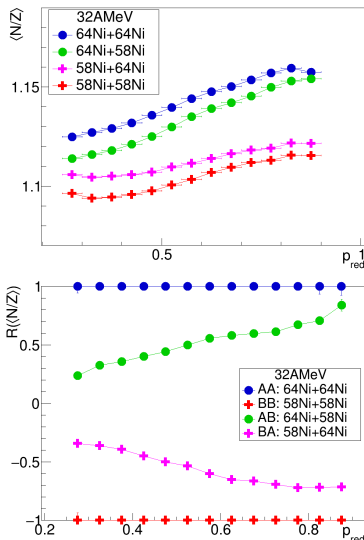
$$R(X) = \frac{2X_i - X_{AA} - X_{BB}}{X_{AA} - X_{BB}}$$

$R(X) = \pm 1 \rightarrow$ non eq.

$R(X_{AB}) = R(X_{BA}) \rightarrow$ equil.

where $i = AA, AB, BA, BB$ and X is an isospin sensitive observable (e.g. $\langle N/Z \rangle_{QP}$).

- Both asymmetric "branches" driven towards each other for low p_{red} (i.e., low b_{red})



QP evaporation channel in Ni+Ni collisions

Isospin diffusion: $\langle N/Z \rangle$ of the QP remnant

Evolution of $\langle N/Z \rangle$ of the QP remnant with centrality \rightarrow **evidence of isospin diffusion**

Isospin transport ratio: can highlight the effect, bypassing the effects acting similarly on the four systems (F. Rami et al., Phys. Rev. Lett. 84, 1120 (2000))

Given $A = {}^{64}\text{Ni}$, $B = {}^{58}\text{Ni}$:

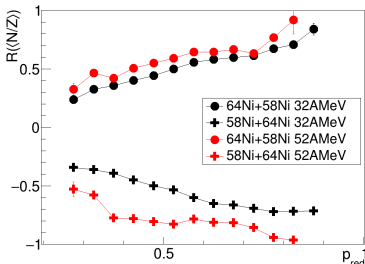
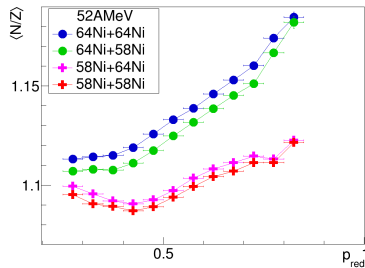
$$R(X) = \frac{2X_i - X_{AA} - X_{BB}}{X_{AA} - X_{BB}}$$

$R(X) = \pm 1 \rightarrow$ non eq.

$R(X_{AB}) = R(X_{BA}) \rightarrow$ equil.

where $i = AA, AB, BA, BB$ and X is an isospin sensitive observable (e.g. $\langle N/Z \rangle_{QP}$).

- Both asymmetric “branches” driven towards each other for low p_{red} (i.e., low b_{red})
- Comparison 32 – 52 MeV/nucl.:
higher degree of equilibration at 32 MeV/nucl.
C.Ciampi et al., Phys. Rev. C 106, 024603 (2022)



QP evaporation channel in Ni+Ni collisions

Isospin diffusion: $\langle N/Z \rangle$ of the QP remnant

Evolution of $\langle N/Z \rangle$ of the QP remnant with centrality \rightarrow **evidence of isospin diffusion**

Isospin transport ratio: can highlight the effect, bypassing the effects acting similarly on the four systems (F. Rami et al., Phys. Rev. Lett. 84, 1120 (2000))

Given $A = {}^{64}\text{Ni}$, $B = {}^{58}\text{Ni}$:

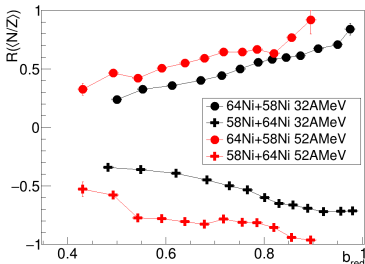
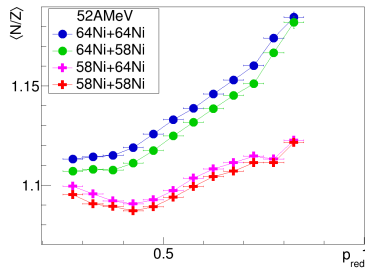
$$R(X) = \frac{2X_i - X_{AA} - X_{BB}}{X_{AA} - X_{BB}}$$

$R(X) = \pm 1 \rightarrow$ non eq.

$R(X_{AB}) = R(X_{BA}) \rightarrow$ equil.

where $i = AA, AB, BA, BB$ and X is an isospin sensitive observable (e.g. $\langle N/Z \rangle_{QP,red}$).

- Both asymmetric “branches” driven towards each other for low p_{red} (i.e., low b_{red})
- Comparison 32 – 52 MeV/nucl.:
higher degree of equilibration at 32 MeV/nucl.
C.Ciampi et al., Phys. Rev. C 106, 024603 (2022)



Ternary output channel

QP fission events

Events with $M_{Z \geq 5} = 2$ include fission events, with both QP fragments detected:

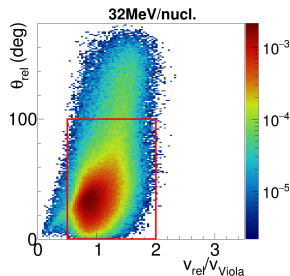
Ternary output channel

QP fission events

Events with $M_{Z \geq 5} = 2$ include fission events, with both QP fragments detected:

→ discard “spurious” QP+QT events:
correlation relative angle θ_{rel} vs relative velocity v_{rel} of the two fragments $Z \geq 5$

⇒ $\theta_{rel} < 90^\circ$ and v_{rel} cond. depending on E_{beam}



Ternary output channel

QP fission events

Events with $M_{Z \geq 5} = 2$ include fission events, with both QP fragments detected:

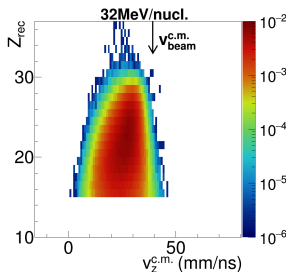
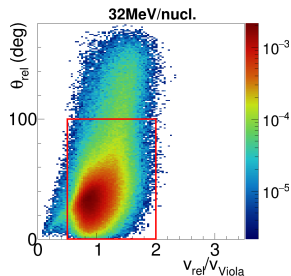
→ discard “spurious” QP+QT events:
correlation relative angle θ_{rel} vs relative velocity v_{rel} of the two fragments $Z \geq 5$

⇒ $\theta_{rel} < 90^\circ$ and v_{rel} cond. depending on E_{beam}

We also require:

- charge of the reconstructed QP

$$Z_{rec} = Z_H + Z_L \geq 15$$



Ternary output channel

QP fission events

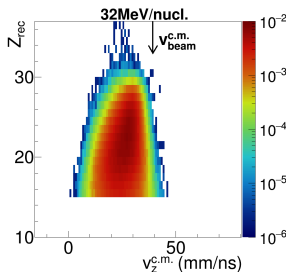
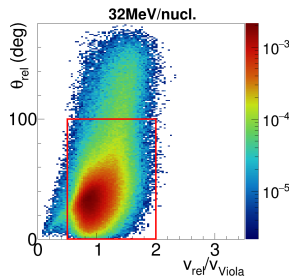
Events with $M_{Z \geq 5} = 2$ include fission events, with both QP fragments detected:

→ discard “spurious” QP+QT events:
correlation relative angle θ_{rel} vs relative velocity v_{rel} of the two fragments $Z \geq 5$

⇒ $\theta_{rel} < 90^\circ$ and v_{rel} cond. depending on E_{beam}

We also require:

- charge of the reconstructed QP
 $Z_{rec} = Z_H + Z_L \geq 15$
→ the “reconstructed” QP is compatible with a forward emitted heavy QP-like fragment



Ternary output channel

QP fission events

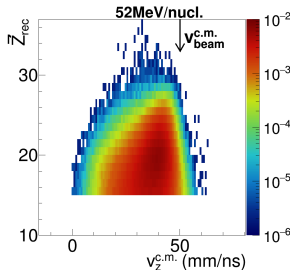
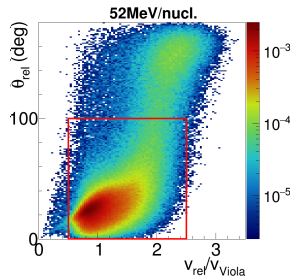
Events with $M_{Z \geq 5} = 2$ include fission events, with both QP fragments detected:

→ discard “spurious” QP+QT events:
correlation relative angle θ_{rel} vs relative velocity v_{rel} of the two fragments $Z \geq 5$

⇒ $\theta_{rel} < 90^\circ$ and v_{rel} cond. depending on E_{beam}

We also require:

- charge of the reconstructed QP
 $Z_{rec} = Z_H + Z_L \geq 15$
→ the “reconstructed” QP is compatible with a forward emitted heavy QP-like fragment
- for the isospin analysis, both A identified
⇒ both $Z \geq 5$ fragments must be in FAZIA



QP breakup channel in Ni+Ni collisions

Channel selection: dynamical or statistical fission? (I)

Set of events compatible with a QP fission process \rightarrow *of which kind?*

QP breakup channel in Ni+Ni collisions

Channel selection: dynamical or statistical fission? (I)

Set of events compatible with a QP fission process \rightarrow *of which kind?*

Statistical fission

- Slow deexcitation process, driven by collective phenomena

Dynamical fission

- Fast process ($\sim 200 - 300$ fm/c), driven by reaction dynamics

QP breakup channel in Ni+Ni collisions

Channel selection: dynamical or statistical fission? (I)

Set of events compatible with a QP fission process → *of which kind?*

Statistical fission

- Slow deexcitation process, driven by collective phenomena
- Isotropic angular distribution of the two fission fragments on the reaction plane

Dynamical fission

- Fast process ($\sim 200 - 300$ fm/c), driven by reaction dynamics
- More aligned configurations observed for larger mass asymmetries of the split

QP breakup channel in Ni+Ni collisions

Channel selection: dynamical or statistical fission? (I)

Set of events compatible with a QP fission process \rightarrow *of which kind?*

Statistical fission

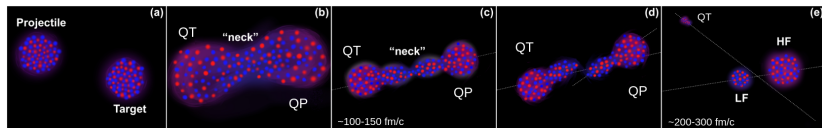
- Slow deexcitation process, driven by collective phenomena
- Isotropic angular distribution of the two fission fragments on the reaction plane

Dynamical fission

- Fast process ($\sim 200 - 300$ fm/c), driven by reaction dynamics
- More aligned configurations observed for larger mass asymmetries of the split

According to a possible interpretation of the dynamical fission:

- QP, QT separate featuring a strong deformation + angular momentum
- Prompt breakup \rightarrow formation of a Light Fragment (LF, from the neck side) and a Heavy Fragment (HF) \rightarrow **asymmetric**
- **Fast process** \rightarrow LF emitted towards CM \rightarrow **anisotropic**



adapted from A. Rodriguez Manso et al., PRC 95, 044604 (2017)

QP breakup channel in Ni+Ni collisions

Channel selection: dynamical or statistical fission? (II)

Experimental data: check the **asymmetry** and the **anisotropy** of the emission of the two fission fragments. We exploit:

QP breakup channel in Ni+Ni collisions

Channel selection: dynamical or statistical fission? (II)

Experimental data: check the **asymmetry** and the **anisotropy** of the emission of the two fission fragments. We exploit:

- Mass asymmetry HF-LF:

$$\eta = \frac{A_H - A_L}{A_{rec}}$$

low η : symmetric split

high η : asymmetric split

QP breakup channel in Ni+Ni collisions

Channel selection: dynamical or statistical fission? (II)

Experimental data: check the **asymmetry** and the **anisotropy** of the emission of the two fission fragments. We exploit:

- Mass asymmetry HF-LF:

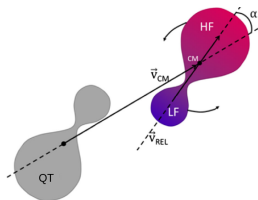
$$\eta = \frac{A_H - A_L}{A_{rec}}$$

low η : symmetric split

high η : asymmetric split

- α angle between the QP-QT separation axis (\vec{v}_{QP-rec}) and the breakup axis (\vec{v}_{rel})

$$\alpha = \arccos\left(\frac{\mathbf{v}_{QP} \cdot \mathbf{v}_{rel}}{|\mathbf{v}_{QP}| |\mathbf{v}_{rel}|}\right)$$



QP breakup channel in Ni+Ni collisions

Channel selection: dynamical or statistical fission? (II)

Experimental data: check the **asymmetry** and the **anisotropy** of the emission of the two fission fragments. We exploit:

- Mass asymmetry HF-LF:

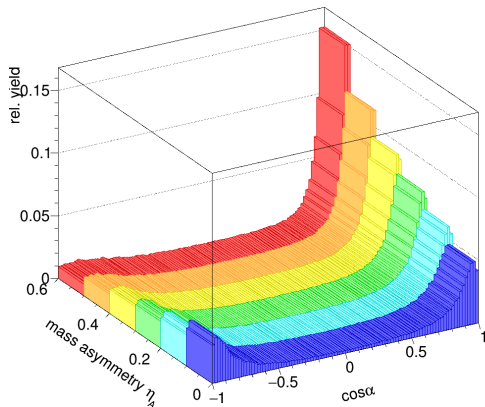
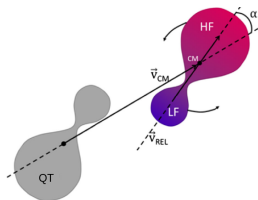
$$\eta = \frac{A_H - A_L}{A_{rec}}$$

low η : symmetric split

high η : asymmetric split

- α angle between the QP-QT separation axis (\vec{v}_{QP-rec}) and the breakup axis (\vec{v}_{rel})

$$\alpha = \arccos\left(\frac{\mathbf{v}_{QP} \cdot \mathbf{v}_{rel}}{|\mathbf{v}_{QP}| |\mathbf{v}_{rel}|}\right)$$



In the asymmetric configuration the backward emission of the LF is favoured, as expected for the dynamical fission

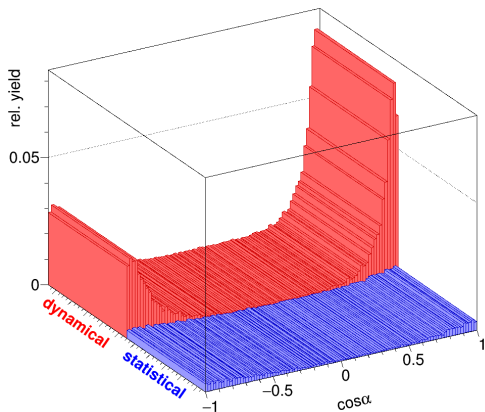
QP breakup channel in Ni+Ni collisions

Channel selection: dynamical or statistical fission? (III)

AMD+GEMINI calculations: check directly “how **fast**” the fission process is.

Dynamical fission → the fragments are present at 500 fm/c (end of AMD calc.)

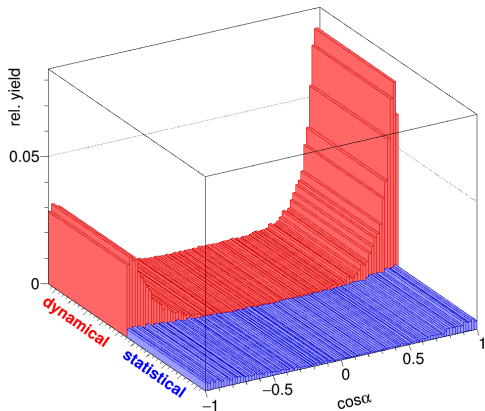
Statistical fission → the fragments are produced by GEMINI



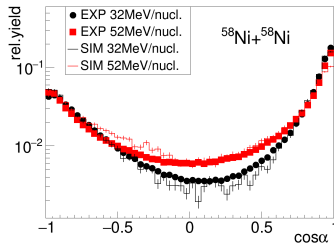
QP breakup channel in Ni+Ni collisions

Channel selection: dynamical or statistical fission? (III)

AMD+GEMINI calculations: check directly “how **fast**” the fission process is.
Dynamical fission → the fragments are present at 500 fm/c (end of AMD calc.)
Statistical fission → the fragments are produced by GEMINI



According to AMD+GEMINI++
about 90% (85%) of the fission events
are dynamical for the reactions
at 32 (52) MeV/nucleon.

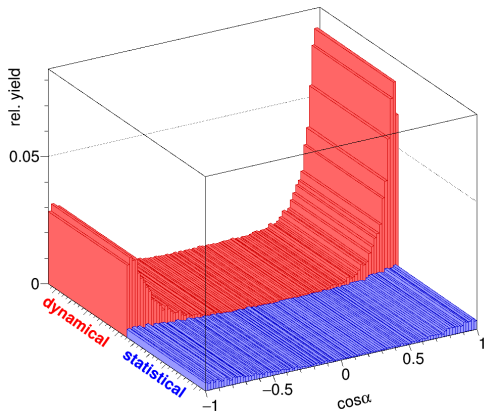


The α and η distributions are quite nicely reproduced.

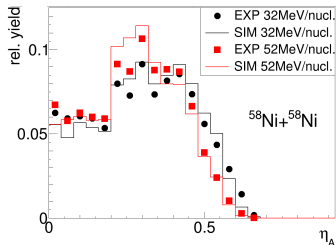
QP breakup channel in Ni+Ni collisions

Channel selection: dynamical or statistical fission? (III)

AMD+GEMINI calculations: check directly “how fast” the fission process is.
Dynamical fission → the fragments are present at 500 fm/c (end of AMD calc.)
Statistical fission → the fragments are produced by GEMINI



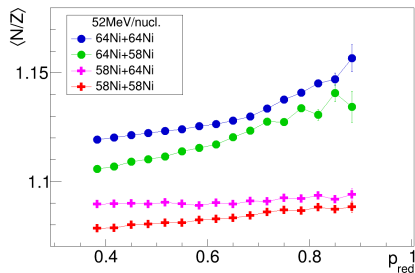
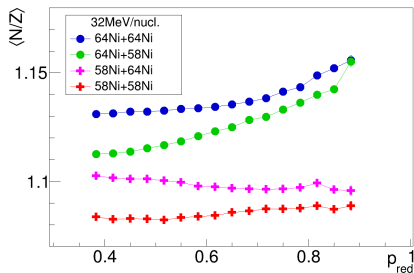
According to AMD+GEMINI++
about 90% (85%) of the fission events
are dynamical for the reactions
at 32 (52) MeV/nucl.



The α and η distributions are quite nicely reproduced.

QP breakup channel in Ni+Ni collisions

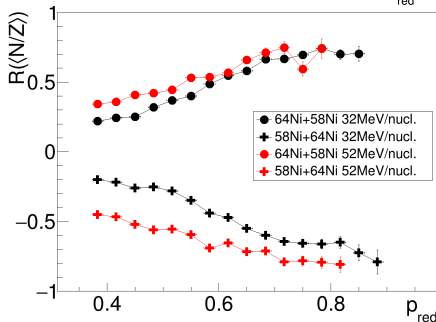
Isospin characteristics



Similarly to what found in the QPr channel, the **isospin diffusion** effect is visible also on the characteristics of the

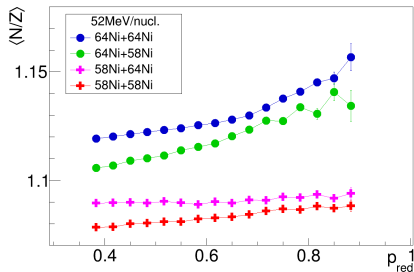
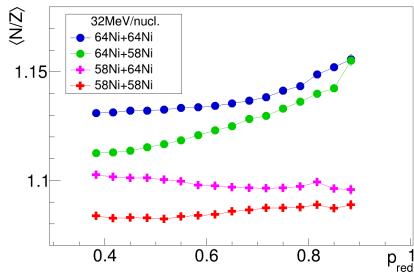
QP reconstructed from the two breakup fragments in the QPb channel.

The comparison between the two E_{beam} leads to the same observation: stronger equilibration for lower E_{beam} .

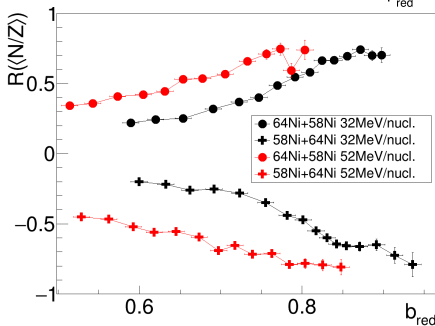


QP breakup channel in Ni+Ni collisions

Isospin characteristics

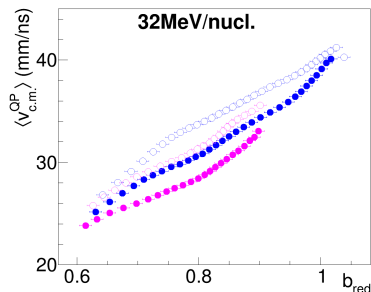


Similarly to what found in the QPr channel, the **isospin diffusion** effect is visible also on the characteristics of the QP reconstructed from the two breakup fragments in the QPb channel. The comparison between the two E_{beam} leads to the same observation: stronger equilibration for lower E_{beam} .



QP breakup channel in Ni+Ni collisions

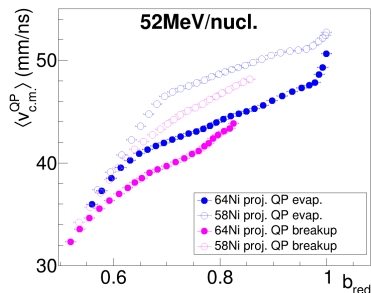
Comparison with the evaporative channel: first overview



Some basic differences are already evident in the measured general properties of the QP (residue or reconstructed) in the two channels.

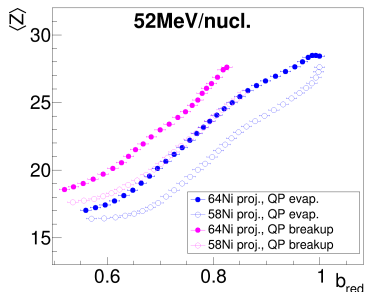
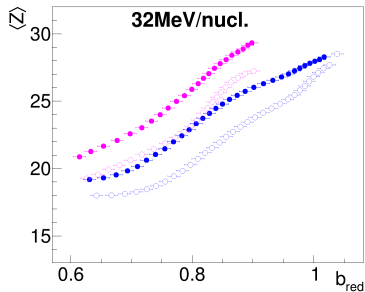
Comparison of $\langle v_{cm}^{QP} \rangle$:

- fissioning QP slower than non-fissioning one



QP breakup channel in Ni+Ni collisions

Comparison with the evaporative channel: first overview



Some basic differences are already evident in the measured general properties of the QP (residue or reconstructed) in the two channels.

Comparison of $\langle v_{cm}^{QP} \rangle$:

- fissioning QP slower than non-fissioning one

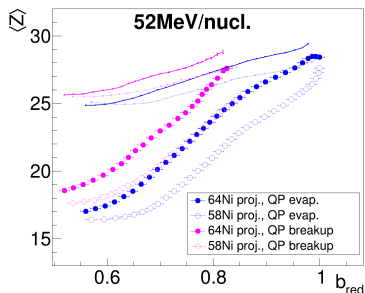
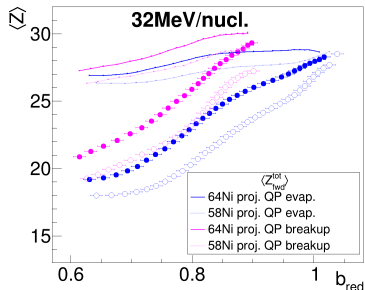
Comparison of $\langle Z^{QP} \rangle$:

- reconstructed QP is $\sim 2-3$ charge units heavier than the remnant

n.b. the primary fragments produced in the two channels may evolve differently in the statistical phase

QP breakup channel in Ni+Ni collisions

Comparison with the evaporative channel: first overview



Some basic differences are already evident in the measured general properties of the QP (residue or reconstructed) in the two channels.

Comparison of $\langle v_{\text{cm}}^{\text{QP}} \rangle$:

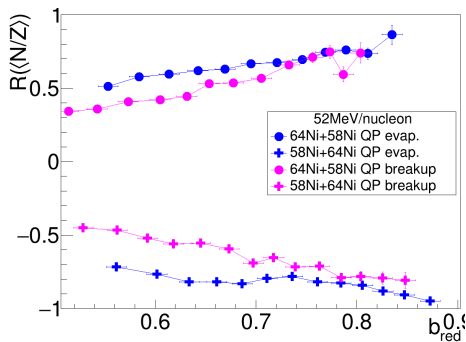
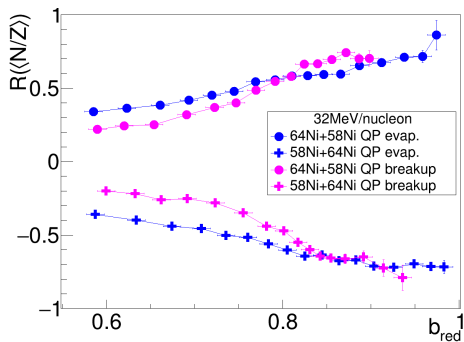
- fissioning QP slower than non-fissioning one

Comparison of $\langle Z^{\text{QP}} \rangle$:

- reconstructed QP is $\sim 2-3$ charge units heavier than the remnant
- n.b.* the primary fragments produced in the two channels may evolve differently in the statistical phase
- average total charge detected in the forward hemisphere $\langle Z_{\text{fwd}}^{\text{tot}} \rangle$ for the breakup channel is still ~ 1 charge unit larger

QP breakup channel in Ni+Ni collisions

Comparison with the evaporative channel: isospin characteristics

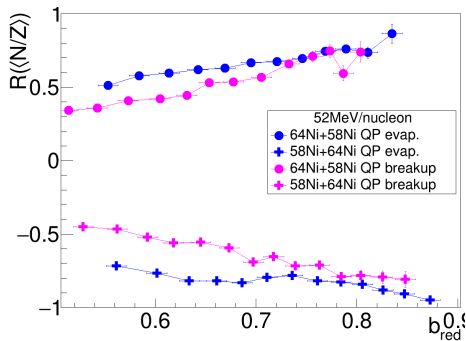
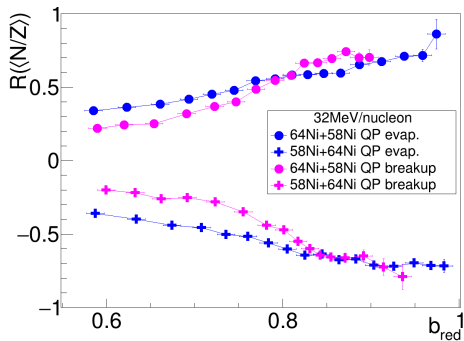


At both energies, for the same reaction centrality a higher degree of isospin equilibration is obtained in the breakup channel than in the evaporative one.

The QP breakup channel seems to select a set of events where a stronger role has been played by the isospin diffusion between projectile and target.

QP breakup channel in Ni+Ni collisions

Comparison with the evaporative channel: isospin characteristics



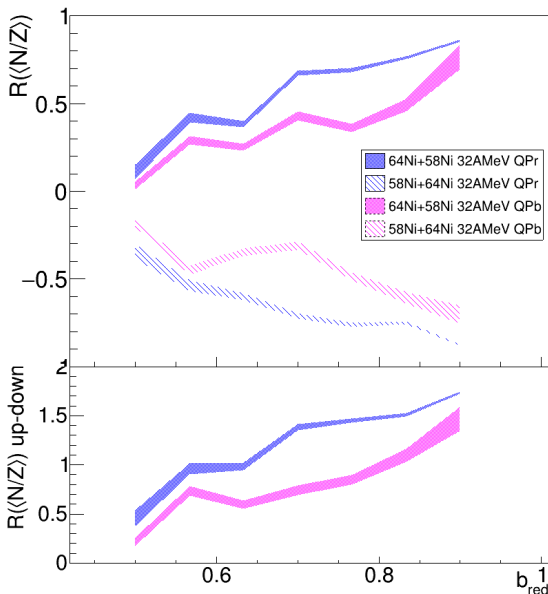
At both energies, for the same reaction centrality a higher degree of isospin equilibration is obtained in the breakup channel than in the evaporative one.

The QP breakup channel seems to select a set of events where a stronger role has been played by the isospin diffusion between projectile and target.

Are we indirectly selecting some events in the tail of the distribution of some parameter related to the reaction dynamics?

QP breakup channel in Ni+Ni collisions

What does the model predict?



AMD+GEM++ simulations

Analysis of the unfiltered simulated datasets (adapting the selection criteria)

→ exclude any possible role of the apparatus acceptance

The stronger isospin equilibration in the breakup channel is visible also in AMD+GEMINI++.

→ track down the differences in the two dynamical scenarios

QP breakup channel in Ni+Ni collisions

A possible interpretation

QP evaporation event



QP breakup event

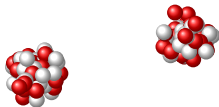


A possible semiclassical interpretation:

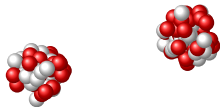
QP breakup channel in Ni+Ni collisions

A possible interpretation

QP evaporation event



QP breakup event



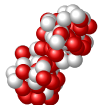
A possible semiclassical interpretation:

- for the same entrance channel conditions

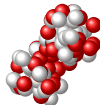
QP breakup channel in Ni+Ni collisions

A possible interpretation

QP evaporation event



QP breakup event



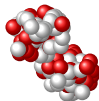
A possible semiclassical interpretation:

- for the same entrance channel conditions (system, E_{beam} , b)

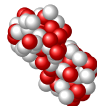
QP breakup channel in Ni+Ni collisions

A possible interpretation

QP evaporation event



QP breakup event



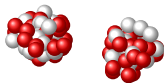
A possible semiclassical interpretation:

- for the same entrance channel conditions (system, E_{beam} , b)
- in the QP breakup channel we may be indirectly selecting longer QP-QT contact times during the interaction phase

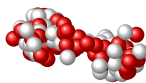
QP breakup channel in Ni+Ni collisions

A possible interpretation

QP evaporation event



QP breakup event



A possible semiclassical interpretation:

- for the same entrance channel conditions (system, E_{beam} , b)
- in the QP breakup channel we may be indirectly selecting longer QP-QT contact times during the interaction phase
- leading to more pronounced deformations of the interacting QP+QT

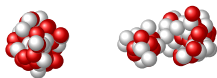
QP breakup channel in Ni+Ni collisions

A possible interpretation

QP evaporation event



QP breakup event



A possible semiclassical interpretation:

- for the same entrance channel conditions (system, E_{beam} , b)
- in the QP breakup channel we may be indirectly selecting longer QP-QT contact times during the interaction phase
- leading to more pronounced deformations of the interacting QP+QT
- with the production of more deformed primary QP (or QT, or both)

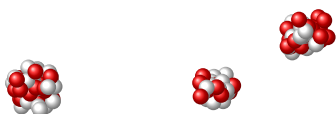
QP breakup channel in Ni+Ni collisions

A possible interpretation

QP evaporation event



QP breakup event

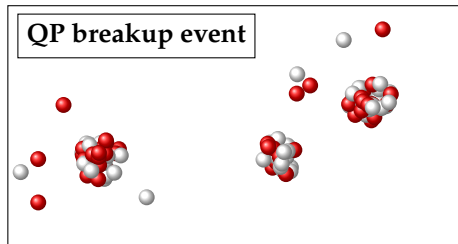
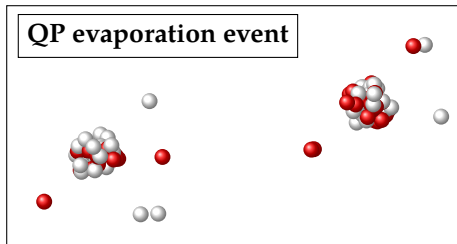


A possible semiclassical interpretation:

- for the same entrance channel conditions (system, E_{beam} , b)
- in the QP breakup channel we may be indirectly selecting longer QP-QT contact times during the interaction phase
- leading to more pronounced deformations of the interacting QP+QT
- with the production of more deformed primary QP (or QT, or both)
- resulting in a QP breakup event

QP breakup channel in Ni+Ni collisions

A possible interpretation



A possible semiclassical interpretation:

- for the same entrance channel conditions (system, E_{beam} , b)
- in the QP breakup channel we may be indirectly selecting longer QP-QT contact times during the interaction phase
- leading to more pronounced deformations of the interacting QP+QT
- with the production of more deformed primary QP (or QT, or both)
- resulting in a QP breakup event
- due to a longer contact time, more isospin equilibration could be achieved

QP-QT interaction time

Extracting the information from AMD

Quite a naive picture (e.g. we do not take into account the density range explored in the contact area), but we could exploit the AMD simulations to extract the contact time information.

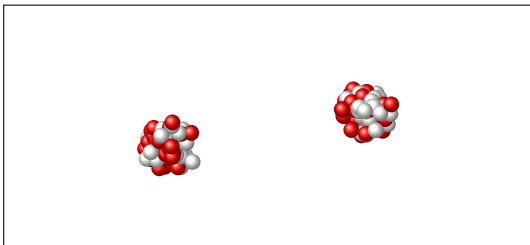


We apply the fragment reconstruction algorithm with a 20fm/c timestep.

QP-QT interaction time

Extracting the information from AMD

Quite a naive picture (e.g. we do not take into account the density range explored in the contact area), but we could exploit the AMD simulations to extract the contact time information.



We apply the fragment reconstruction algorithm with a $20\text{fm}/c$ timestep.

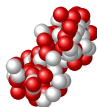
We read the event at each timestep from $0\text{fm}/c$
→ $500\text{fm}/c$, looking for:

QP-QT interaction time

Extracting the information from AMD

Quite a naive picture (e.g. we do not take into account the density range explored in the contact area), but we could exploit the AMD simulations to extract the contact time information.

t_{stick}



We apply the fragment reconstruction algorithm with a 20fm/c timestep.

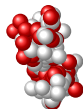
We read the event at each timestep from 0fm/c
→ 500 fm/c, looking for:

t_{stick} first timestep in which only one heavy fragment is found

QP-QT interaction time

Extracting the information from AMD

Quite a naive picture (e.g. we do not take into account the density range explored in the contact area), but we could exploit the AMD simulations to extract the contact time information.



We apply the fragment reconstruction algorithm with a 20fm/c timestep.

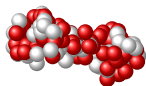
We read the event at each timestep from 0fm/c
→ 500 fm/c, looking for:

t_{stick} first timestep in which only one heavy fragment is found

QP-QT interaction time

Extracting the information from AMD

Quite a naive picture (e.g. we do not take into account the density range explored in the contact area), but we could exploit the AMD simulations to extract the contact time information.



We apply the fragment reconstruction algorithm with a 20fm/c timestep.

We read the event at each timestep from 0fm/c
→ 500 fm/c, looking for:

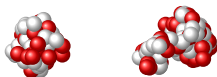
t_{stick} first timestep in which only one heavy fragment is found

QP-QT interaction time

Extracting the information from AMD

Quite a naive picture (e.g. we do not take into account the density range explored in the contact area), but we could exploit the AMD simulations to extract the contact time information.

t_{QP-QT}



We apply the fragment reconstruction algorithm with a 20fm/c timestep.

We read the event at each timestep from 0fm/c
→ 500 fm/c, looking for:

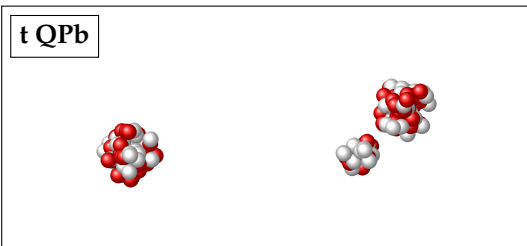
t_{stick} first timestep in which only one heavy fragment is found

t_{QP-QT} first timestep after t_{stick} with at least two heavy fragments
(the characteristics of the QP and QT at this stage are stored as well)

QP-QT interaction time

Extracting the information from AMD

Quite a naive picture (e.g. we do not take into account the density range explored in the contact area), but we could exploit the AMD simulations to extract the contact time information.



We apply the fragment reconstruction algorithm with a 20fm/c timestep.

We read the event at each timestep from 0fm/c
→ 500 fm/c, looking for:

- t_{stick} first timestep in which only one heavy fragment is found
- t_{QP-QT} first timestep after t_{stick} with at least two heavy fragments (the characteristics of the QP and QT at this stage are stored as well)
- $t_{breakup}$ first timestep $\geq t_{QP-QT}$ with two heavy fragments forward (QPb) or backward (QTb) (presently not used, but stored for further studies)

QP-QT interaction time

Extracting the information from AMD

Quite a naive picture (e.g. we do not take into account the density range explored in the contact area), but we could exploit the AMD simulations to extract the contact time information.



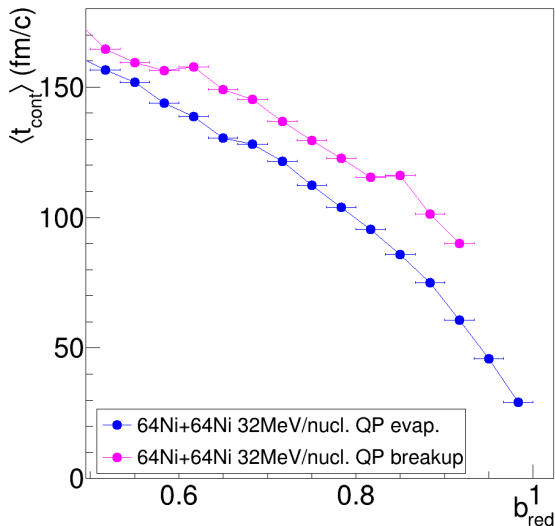
We apply the fragment reconstruction algorithm with a 20fm/c timestep.

We read the event at each timestep from 0fm/c
→ 500 fm/c, looking for:

- t_{stick} first timestep in which only one heavy fragment is found
- t_{QP-QT} first timestep after t_{stick} with at least two heavy fragments (the characteristics of the QP and QT at this stage are stored as well)
- $t_{breakup}$ first timestep $\geq t_{QP-QT}$ with two heavy fragments forward (QPb) or backward (QTb) (presently not used, but stored for further studies)

QP-QT interaction time

Slightly longer contact times

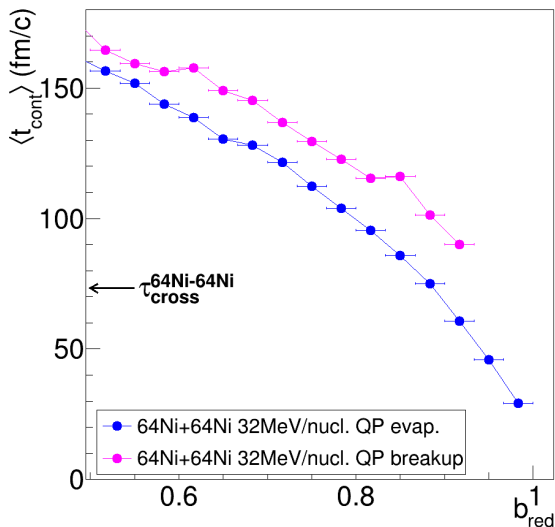


Analysis in 4π :

- Slightly longer contact times are on average indirectly selected in the breakup channel with respect to the evaporative one

QP-QT interaction time

Slightly longer contact times

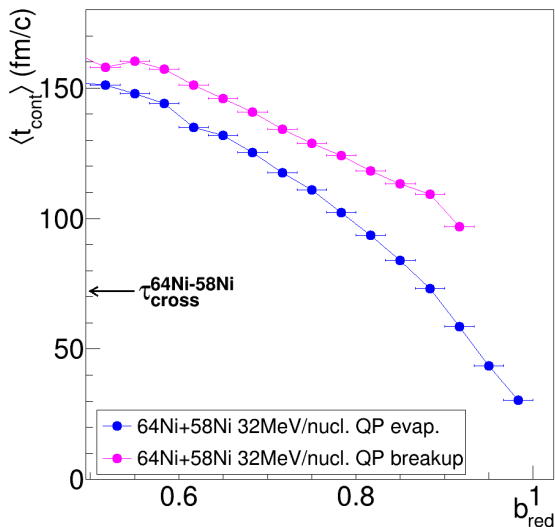


Analysis in 4π :

- Slightly longer contact times are on average indirectly selected in the breakup channel with respect to the evaporative one
- Reliability of $\langle t_{\text{cont}} \rangle$:
$$\tau_{\text{cross}} = 2R_0(A_p^{1/3} + A_t^{1/3})/v_{\text{beam}}^{\text{lab}}$$
 - reasonable $\langle t_{\text{cont}} \rangle$ vs b_{red}

QP-QT interaction time

Slightly longer contact times



Analysis in 4π :

- Slightly longer contact times are on average indirectly selected in the breakup channel with respect to the evaporative one

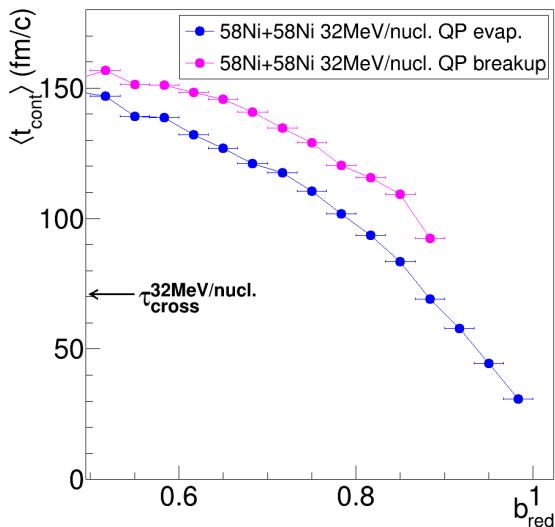
- Reliability of $\langle t_{\text{cont}} \rangle$:

$$\tau_{\text{cross}} = 2R_0(A_p^{1/3} + A_t^{1/3})/v_{\text{beam}}^{\text{lab}}$$

- reasonable $\langle t_{\text{cont}} \rangle$ vs b_{red}
- scales correctly with the system

QP-QT interaction time

Slightly longer contact times

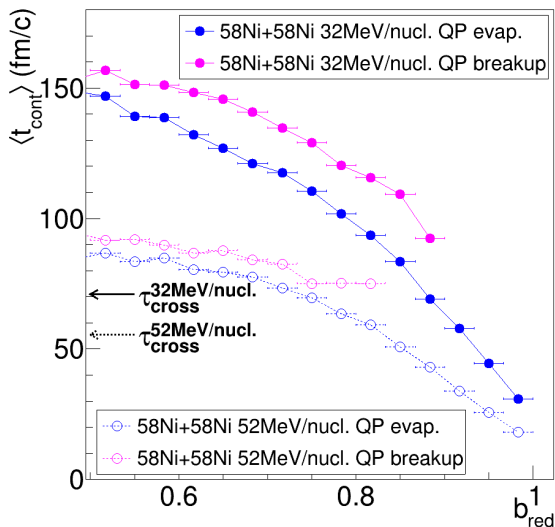


Analysis in 4π :

- Slightly longer contact times are on average indirectly selected in the breakup channel with respect to the evaporative one
- Reliability of $\langle t_{\text{cont}} \rangle$:
 - $\tau_{\text{cross}} = 2R_0(A_p^{1/3} + A_t^{1/3})/v_{\text{beam}}^{\text{lab}}$
 - reasonable $\langle t_{\text{cont}} \rangle$ vs b_{red}
 - scales correctly with the system

QP-QT interaction time

Slightly longer contact times



Analysis in 4π :

- Slightly longer contact times are on average indirectly selected in the breakup channel with respect to the evaporative one

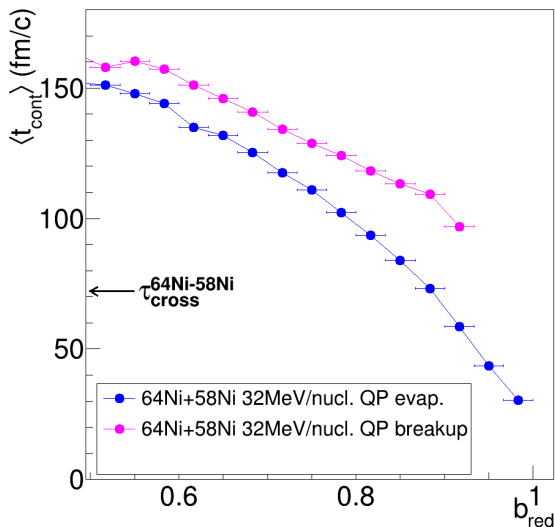
- Reliability of $\langle t_{\text{cont}} \rangle$:

$$\tau_{\text{cross}} = 2R_0(A_p^{1/3} + A_t^{1/3})/v_{\text{beam}}^{\text{lab}}$$

- reasonable $\langle t_{\text{cont}} \rangle$ vs b_{red}
- scales correctly with the system and with E_{beam}

QP-QT interaction time

Slightly longer contact times

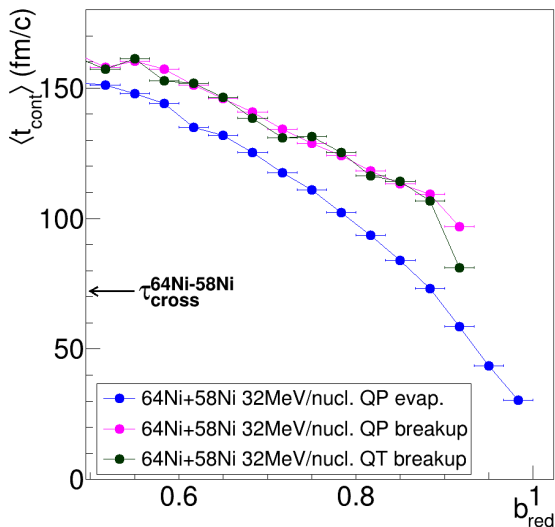


Analysis in 4π :

- Slightly longer contact times are on average indirectly selected in the breakup channel with respect to the evaporative one
- Reliability of $\langle t_{\text{cont}} \rangle$:
$$\tau_{\text{cross}} = 2R_0(A_p^{1/3} + A_t^{1/3})/v_{\text{beam}}^{\text{lab}}$$
 - reasonable $\langle t_{\text{cont}} \rangle$ vs b_{red}
 - scales correctly with the system and with E_{beam}
- Similar t_{cont} are related to the breakup of the QP

QP-QT interaction time

Slightly longer contact times

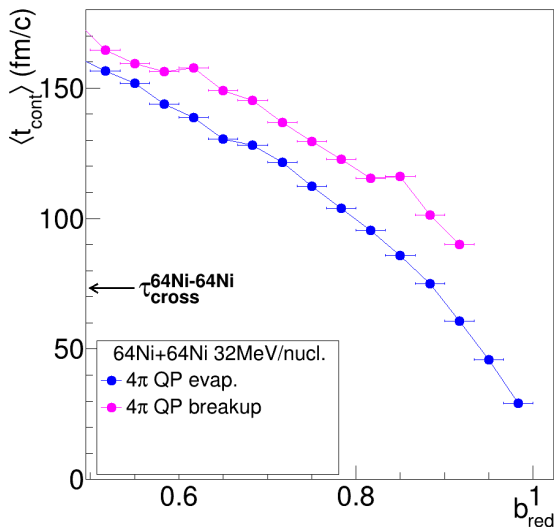


Analysis in 4π :

- Slightly longer contact times are on average indirectly selected in the breakup channel with respect to the evaporative one
- Reliability of $\langle t_{\text{cont}} \rangle$:
$$\tau_{\text{cross}} = 2R_0(A_p^{1/3} + A_t^{1/3})/v_{\text{beam}}^{\text{lab}}$$
 - reasonable $\langle t_{\text{cont}} \rangle$ vs b_{red}
 - scales correctly with the system and with E_{beam}
- Similar t_{cont} are related to the breakup of the QP and QT

QP-QT interaction time

Slightly longer contact times



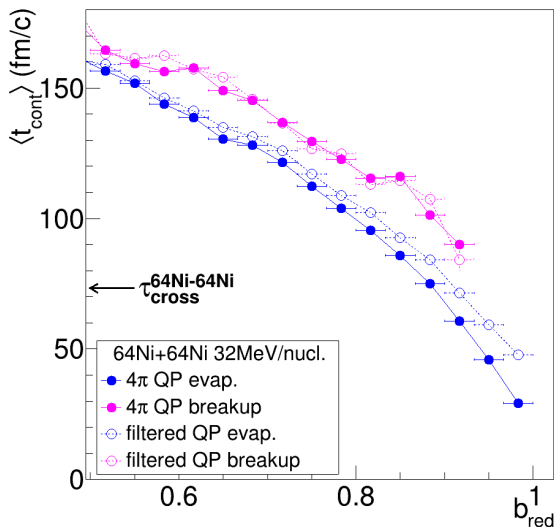
Analysis in 4 π :

- Slightly longer contact times are on average indirectly selected in the breakup channel with respect to the evaporative one
- Reliability of $\langle t_{\text{cont}} \rangle$:
$$\tau_{\text{cross}} = 2R_0(A_p^{1/3} + A_t^{1/3})/v_{\text{beam}}^{\text{lab}}$$
 - reasonable $\langle t_{\text{cont}} \rangle$ vs b_{red}
 - scales correctly with the system and with E_{beam}
- Similar t_{cont} are related to the breakup of the QP and QT

Analysis after filter:

QP-QT interaction time

Slightly longer contact times



Analysis in 4 π :

- Slightly longer contact times are on average indirectly selected in the breakup channel with respect to the evaporative one
- Reliability of $\langle t_{\text{cont}} \rangle$:
$$\tau_{\text{cross}} = 2R_0(A_p^{1/3} + A_t^{1/3})/v_{\text{beam}}^{\text{lab}}$$
 - reasonable $\langle t_{\text{cont}} \rangle$ vs b_{red}
 - scales correctly with the system and with E_{beam}
- Similar t_{cont} are related to the breakup of the QP and QT

Analysis after filter:

- Small t_{cont} variation only for the evaporative channel, but still longer for QP breakup

Summary and future perspectives

Summary

- INDRA-FAZIA E789: $^{64,58}\text{Ni} + ^{64,58}\text{Ni}$ at 32 and 52 MeV/nucl.
- QP-QT isospin equilibration in the two reaction channels:
 - clear relaxation of the isospin imbalance in asymmetric systems
 - stronger equilibration at lower beam energy

Summary and future perspectives

Summary

- INDRA-FAZIA E789: $^{64,58}\text{Ni} + ^{64,58}\text{Ni}$ at 32 and 52 MeV/nucl.
- QP-QT isospin equilibration in the two reaction channels:
 - clear relaxation of the isospin imbalance in asymmetric systems
 - stronger equilibration at lower beam energy
 - stronger equilibration in the breakup than in the evaporative channel

Summary and future perspectives

Summary

- INDRA-FAZIA E789: $^{64,58}\text{Ni} + ^{64,58}\text{Ni}$ at 32 and 52 MeV/nucl.
- QP-QT isospin equilibration in the two reaction channels:
 - clear relaxation of the isospin imbalance in asymmetric systems
 - stronger equilibration at lower beam energy
 - *stronger equilibration in the breakup than in the evaporative channel*
- Interpretation based on *longer QP-QT contact times indirectly selected in the breakup output*, supported by AMD calculations

Summary and future perspectives

Summary

- INDRA-FAZIA E789: $^{64,58}\text{Ni} + ^{64,58}\text{Ni}$ at 32 and 52 MeV/nucleon
- QP-QT isospin equilibration in the two reaction channels:
 - clear relaxation of the isospin imbalance in asymmetric systems
 - stronger equilibration at lower beam energy
 - stronger equilibration in the breakup than in the evaporative channel
- Interpretation based on *longer QP-QT contact times indirectly selected in the breakup output*, supported by AMD calculations

Future perspectives

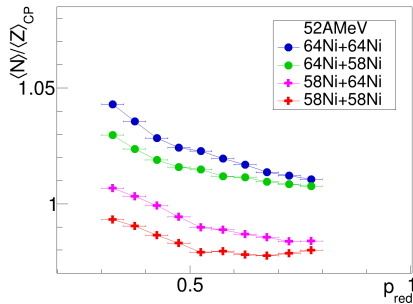
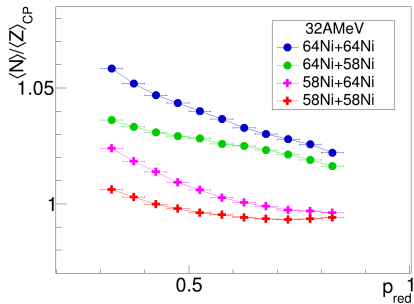
- Study the other dynamical features related to a longer interaction (e.g., density evolution) selected by the breakup channel, as well as the consequences on the sensitivity to the N EoS parametrization
- Isospin equilibration between QP breakup fragments HF and LF
- Detailed comparison with models: AMD and BUU model (S.Mallik et al., J. Phys. G: Nucl. Part. Phys. 49 (2022) 015102)

Thank you!

Backup slides

Isospin diffusion

QPr channel: characteristics of the evaporated particles (I)



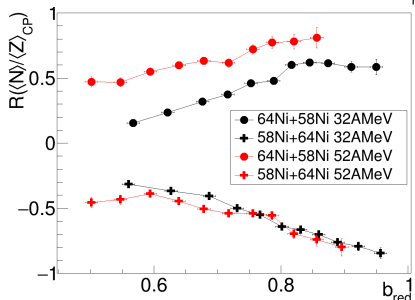
The QP-QT isospin equilibration can be evidenced also on the characteristics of the QP deexcitation emissions.

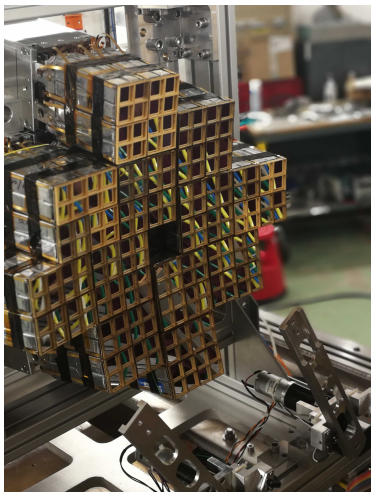
→ e.g., isospin ratio for complex particles forward emitted with respect to the QP remnant.

$$\langle N \rangle / \langle Z \rangle_{CP} = \frac{\sum_i \sum_\nu N_\nu^i}{\sum_i \sum_\nu Z_\nu^i}$$

considering LCPs and IMFs with $A > 1$.

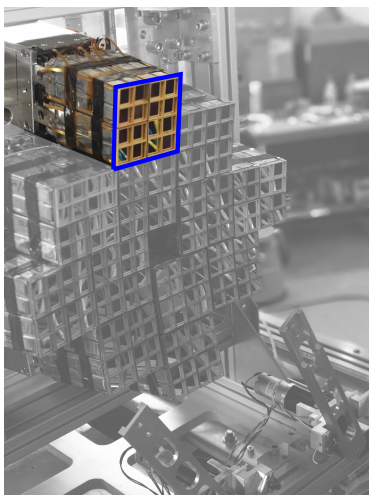
see E. Galichet et al., PRC 79, 064614 (2009)





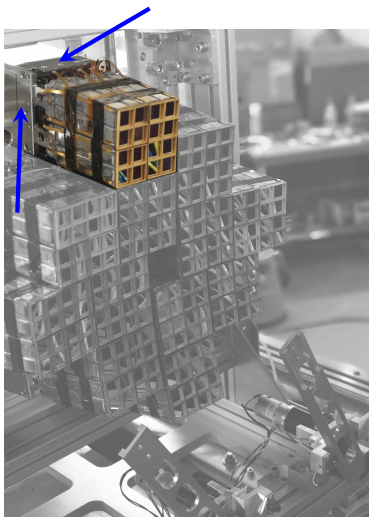
FAZIA (*Forward-angle A and Z Identification Array*): state of the art of ion identification in the Fermi energy domain.

- Result of R&D activities to refine:
 - detector performance
 - digital treatment of signals



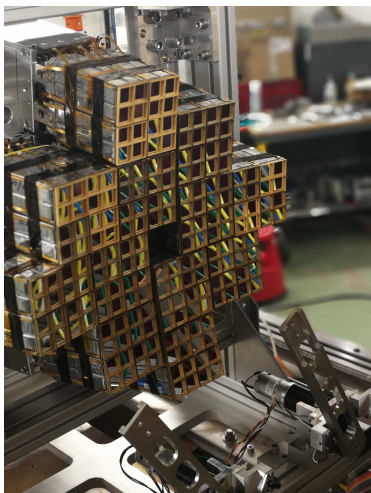
FAZIA (*Forward-angle A and Z Identification Array*): state of the art of ion identification in the Fermi energy domain.

- Result of R&D activities to refine:
 - detector performance
 - digital treatment of signals
- Basic module: **block**, consisting of 16 three stage **telescopes** ($2 \times 2 \text{ cm}^2$ active area):
 - Si1 300 μm thick
 - Si2 500 μm thick
 - CsI(Tl) 10cm thick



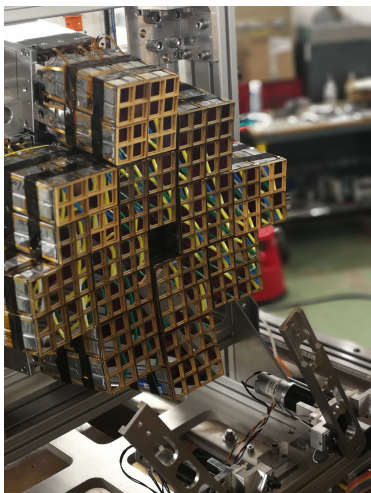
FAZIA (*Forward-angle A and Z Identification Array*): state of the art of ion identification in the Fermi energy domain.

- Result of R&D activities to refine:
 - detector performance
 - digital treatment of signals
 - Basic module: **block**, consisting of 16 three stage **telescopes** ($2 \times 2 \text{ cm}^2$ active area):
 - Si1 300 μm thick
 - Si2 500 μm thick
 - CsI(Tl) 10cm thick
- + read-out electronics for all telescopes.



FAZIA (*Forward-angle A and Z Identification Array*): state of the art of ion identification in the Fermi energy domain.

- Result of R&D activities to refine:
 - detector performance
 - digital treatment of signals
 - Basic module: **block**, consisting of 16 three stage **telescopes** ($2 \times 2 \text{ cm}^2$ active area):
 - Si1 300 μm thick
 - Si2 500 μm thick
 - CsI(Tl) 10cm thick
- + read-out electronics for all telescopes.
- Identification techniques: ΔE -E / PSA
 - Charge discrimination tested up to $Z \sim 55$
 - Mass discrimination up to $Z \sim 25$ / $Z \sim 22$



→ see talks by G. Casini, A. Camaiani

FAZIA (*Forward-angle A and Z Identification Array*): state of the art of ion identification in the Fermi energy domain.

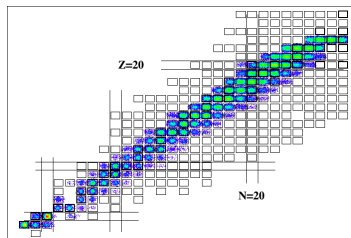
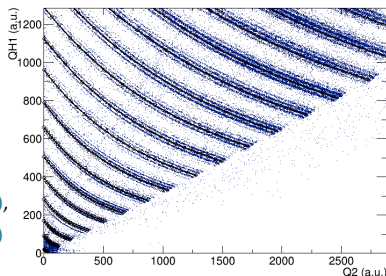
- Result of R&D activities to refine:
 - detector performance
 - digital treatment of signals
- Basic module: **block**, consisting of 16 three stage **telescopes** ($2 \times 2 \text{ cm}^2$ active area):
 - Si1 300 μm thick
 - Si2 500 μm thick
 - CsI(Tl) 10cm thick
- + read-out electronics for all telescopes.
- Identification techniques: ΔE -E / PSA
 - Charge discrimination tested up to $Z \sim 55$
 - Mass discrimination up to $Z \sim 25$ / $Z \sim 22$

FAZIA

The experimental campaigns

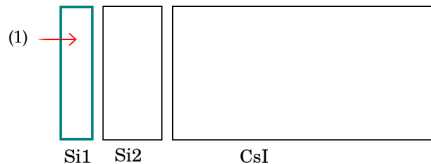
After the R&D phase, the first experimental campaign started at LNS, Catania:

- ISOFAZIA (2015):
 $^{80}\text{Kr}+^{40,48}\text{Ca}$ at 35 MeV/nucl.
S. Piantelli et al., Phys. Rev. C 101, 034613 (2020),
S. Piantelli et al., Phys. Rev. C 103, 014603 (2021)
- FAZIASYM (2015):
 $^{40,48}\text{Ca}+^{40,48}\text{Ca}$ at 35 MeV/nucl.
A. Camaiani et al., Phys. Rev. C 102, 044607 (2020),
A. Camaiani et al., Phys. Rev. C 103, 014605 (2021)
- FAZIACOR (2017):
 $^{20}\text{Ne}, ^{32}\text{S}+^{12}\text{C}$ at 25, 50 MeV/nucl.
C. Frosin et al., Phys. Rev. C 107, 044614 (2023)
→ see talk by A. Camaiani
- FAZIAPRE (2018):
 $^{40,48}\text{Ca}+^{12}\text{C}$ at 25, 40 MeV/nucl.
S. Piantelli et al., Phys. Rev. C 107, 044607 (2023)
- FAZIAZERO (2018):
 $^{12}\text{C}+^{12}\text{C}$ at 62 MeV/nucl.



Experimental setup

Identification techniques



Different identification methods depending on the stopping layer:

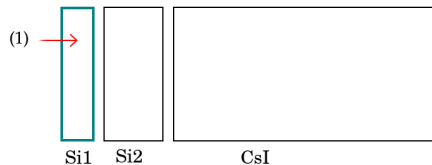
- 1 Si1: PSA-Si

Pulse Shape Analysis: identification of fragments stopped in a detector (e.g. Si1)



Experimental setup

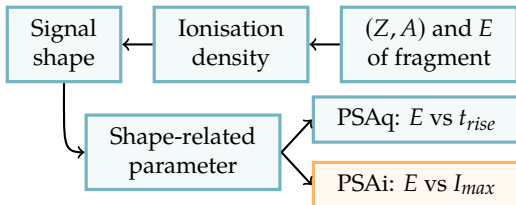
Identification techniques



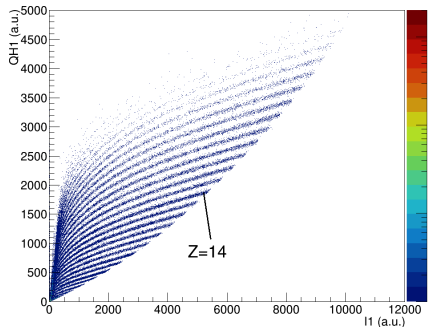
Different identification methods depending on the stopping layer:

- 1 Si: **PSA-Si**

Pulse Shape Analysis: identification of fragments stopped in a detector (e.g. Si1)

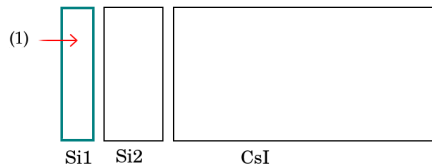


- A good doping uniformity is mandatory
- Si detectors are reverse mounted



Experimental setup

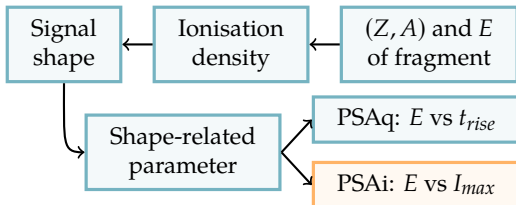
Identification techniques



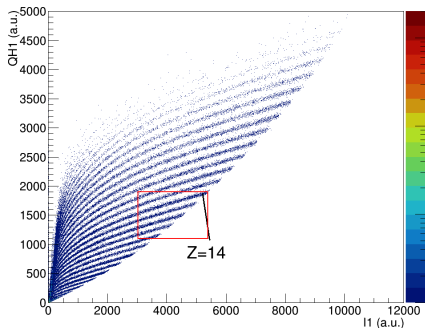
Different identification methods depending on the stopping layer:

- 1 Si: PSA-Si

Pulse Shape Analysis: identification of fragments stopped in a detector (e.g. Si1)

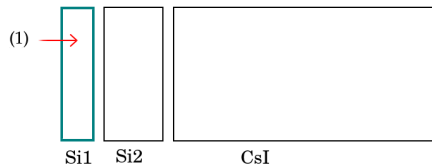


- A good doping uniformity is mandatory
- Si detectors are reverse mounted



Experimental setup

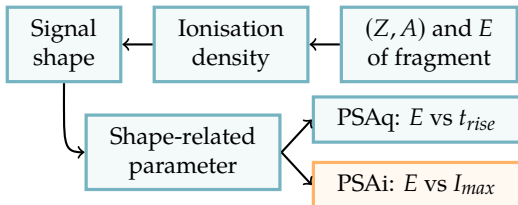
Identification techniques



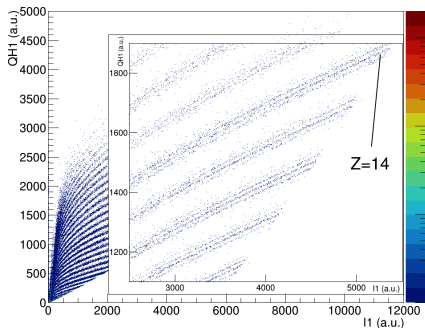
Different identification methods depending on the stopping layer:

- 1 Si: **PSA-Si**

Pulse Shape Analysis: identification of fragments stopped in a detector (e.g. Si1)

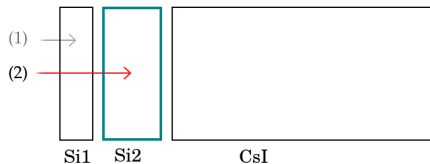


- A good doping uniformity is mandatory
- Si detectors are reverse mounted



Experimental setup

Identification techniques



Different identification methods depending on the stopping layer:

- 1 Si1: PSA-Si
- 2 Si2: ΔE -E Si1-Si2

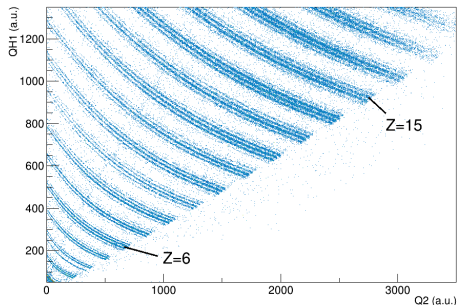
ΔE -E technique: based on the mechanism of kinetic energy dissipation of charged particles in matter → Bethe-Bloch

$$-\frac{dE}{dx} = \frac{4\pi e^4 Z^2}{m_e v^2} N_Z \left[\ln \frac{2m_e v^2}{I} - \ln(1 - \beta^2) - \beta^2 \right]$$

In a non-relativistic approx. ($E_0 = \Delta E + E_{res}$):

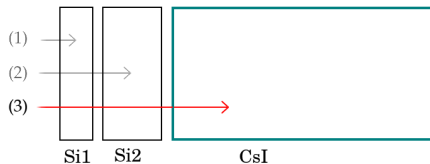
$$\Delta E \propto \frac{Z^2}{v^2} \cdot \Delta x \propto \frac{Z^2 A}{E_0} \cdot \Delta x \Rightarrow \Delta E \cdot E_0 = k Z^2 A$$

Identify the ejectiles stopped in the second stage detector



Experimental setup

Identification techniques



Different identification methods depending on the stopping layer:

- 1 Si1: PSA-Si
- 2 Si2: ΔE -E Si1-Si2
- 3 CsI: ΔE -E Si2-CsI

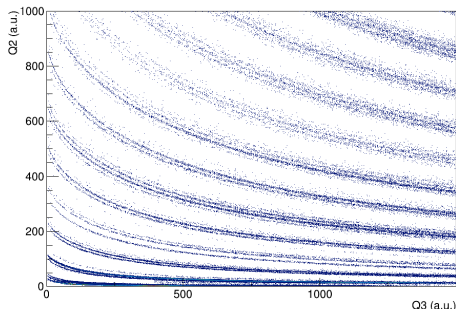
ΔE -E technique: based on the mechanism of kinetic energy dissipation of charged particles in matter \rightarrow Bethe-Bloch

$$-\frac{dE}{dx} = \frac{4\pi e^4 Z^2}{m_e v^2} N_Z \left[\ln \frac{2m_e v^2}{I} - \ln(1 - \beta^2) - \beta^2 \right]$$

In a non-relativistic approx. ($E_0 = \Delta E + E_{res}$):

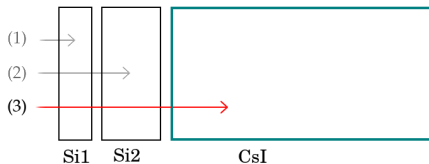
$$\Delta E \propto \frac{Z^2}{v^2} \cdot \Delta x \propto \frac{Z^2 A}{E_0} \cdot \Delta x \Rightarrow \Delta E \cdot E_0 = k Z^2 A$$

Identify the ejectiles stopped in the second stage detector, and also in the third stage



Experimental setup

Identification techniques



Different identification methods depending on the stopping layer:

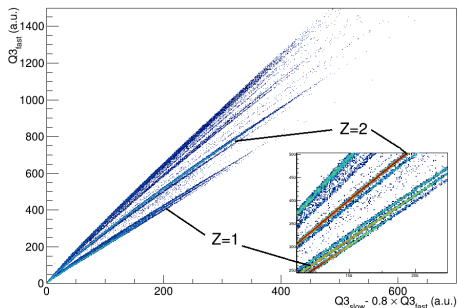
- 1 Si1: PSA-Si
- 2 Si2: ΔE -E Si1-Si2
- 3 CsI: ΔE -E Si2-CsI or **PSA-CsI**

Pulse Shape Analysis in CsI: used for high-energy LCPs.
Intensity of scintillation light:

$$I(t) = I_{fast} \cdot \frac{e^{-t/\tau_{fast}}}{\tau_{fast}} + I_{slow} \cdot \frac{e^{-t/\tau_{slow}}}{\tau_{slow}}$$

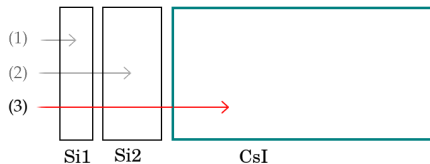
where $\tau_{fast} \sim 700$ ns and $\tau_{slow} \sim 5$ μ s. The ratio I_{fast}/I_{slow} depends on (Z, A) and E of fragment.

Digital electronics: two trapezoidal shapers with different flat top applied to CsI signal.



Experimental setup

Identification techniques



Different identification methods depending on the stopping layer:

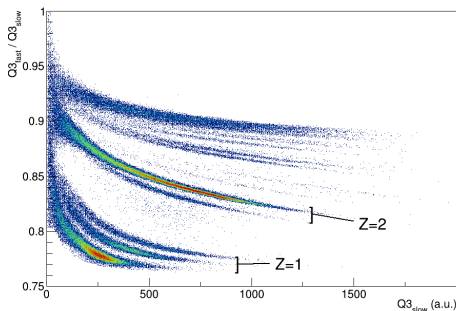
- 1 Si1: PSA-Si
- 2 Si2: ΔE -E Si1-Si2
- 3 CsI: ΔE -E Si2-CsI or PSA-CsI

Pulse Shape Analysis in CsI: used for high-energy LCPs.
Intensity of scintillation light:

$$I(t) = I_{fast} \cdot \frac{e^{-t/\tau_{fast}}}{\tau_{fast}} + I_{slow} \cdot \frac{e^{-t/\tau_{slow}}}{\tau_{slow}}$$

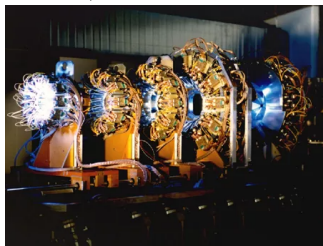
where $\tau_{fast} \sim 700$ ns and $\tau_{slow} \sim 5$ μ s. The ratio I_{fast}/I_{slow} depends on (Z, A) and E of fragment.

Digital electronics: two trapezoidal shapers with different flat top applied to CsI signal.

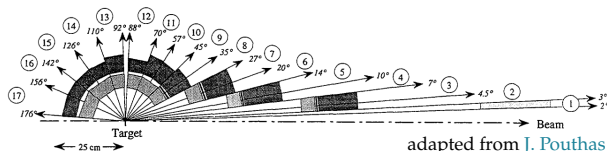


INDRA (*Identification de Noyaux et Détection avec Résolutions Accrues*): highly segmented array for detection and identification of charged products of heavy ion collisions at intermediate energies ($10 < E < 100$ AMeV).

- Original configuration of 17 rings:
 - 1: Si + CsI(Tl)
 - 2-9: Ionisation ch. + Si + CsI(Tl)
 - 10-17: Ionisation ch. + CsI(Tl)
- Charge discrimination up to uranium, mass discrimination up to $Z \sim 4$
 → Electronics upgrade (2020): now up to $Z \sim 10$
 J. D. Frankland et al., *Nuovo Cim. C* 45, 43 (2022)
- Large solid angle coverage (90%) with high granularity (336 modules)



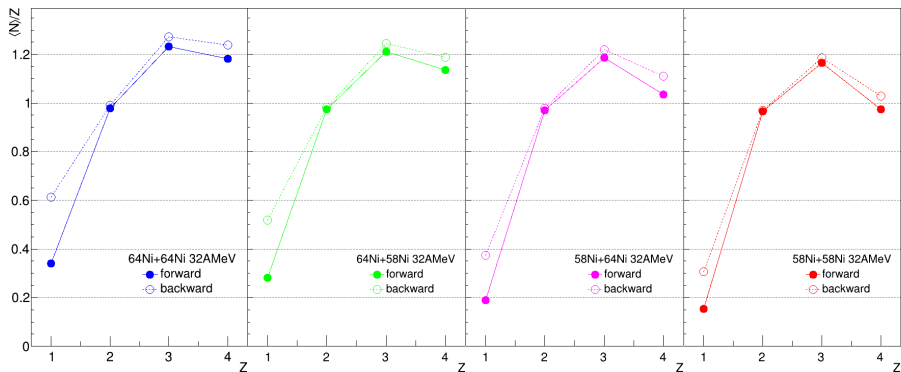
→ see talks by Q. Fable, T. Génard



adapted from J. Pouthas et al., *NIMA* 357, 418 (1995)

Isospin drift

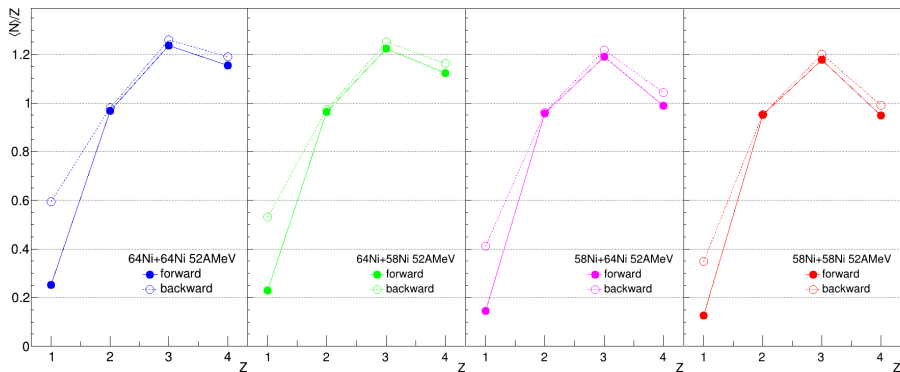
QPr channel: LCPs and IMFs



- We analyse the isospin content of LCPs and IMFs according to their emission pattern, i.e. their orientation with respect to the QP remnant:
 - forward: forward QPr emission of LCPs and IMFs
 - backward: backward QPr emission of LCPs and IMFs, with $v_z^{CM} > 0$
- **Isospin drift** $\rightarrow \langle N \rangle$ for the backward emissions is higher than the forward one. Clean interpretation for symmetric systems.

Isospin drift

QPr channel: LCPs and IMFs

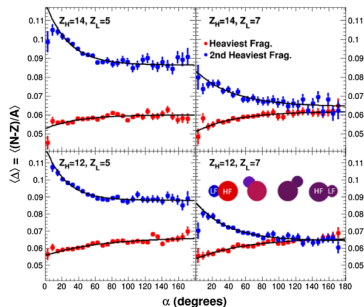


- We analyse the isospin content of LCPs and IMFs according to their emission pattern, i.e. their orientation with respect to the QP remnant:
 - forward: forward QPr emission of LCPs and IMFs
 - backward: backward QPr emission of LCPs and IMFs, with $v_z^{CM} > 0$
- **Isospin drift** $\rightarrow \langle N \rangle$ for the backward emissions is higher than the forward one. Clean interpretation for symmetric systems.

QP breakup channel in Ni+Ni collisions

Recent highlights on dynamical fission

- For a longer time interval elapsed between the QP-QT split and the QP breakup:
 - the degree of isospin equilibration inside the original QP increases
 - the α angle between the separation axis and the breakup axis increases: for a short breakup timescale α can be adopted as a “clock”
- ⇒ *Equilibration chronometry*: extraction of a timescale of isospin equilibration (\sim zs)

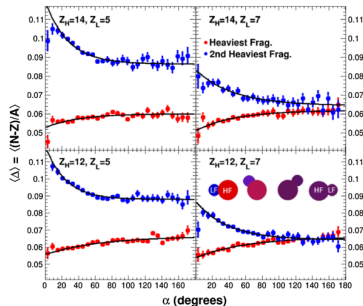
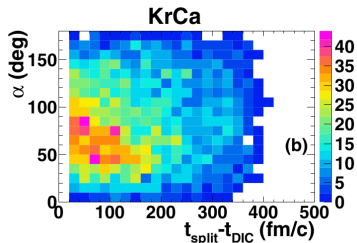


from A. Jedyte et al., PRL118, 062501 (2017)

QP breakup channel in Ni+Ni collisions

Recent highlights on dynamical fission

- For a longer time interval elapsed between the QP-QT split and the QP breakup:
 - the degree of isospin equilibration inside the original QP increases
 - the α angle between the separation axis and the breakup axis increases: for a short breakup timescale α can be adopted as a “clock”
- ⇒ *Equilibration chronometry*: extraction of a timescale of isospin equilibration (\sim zs)



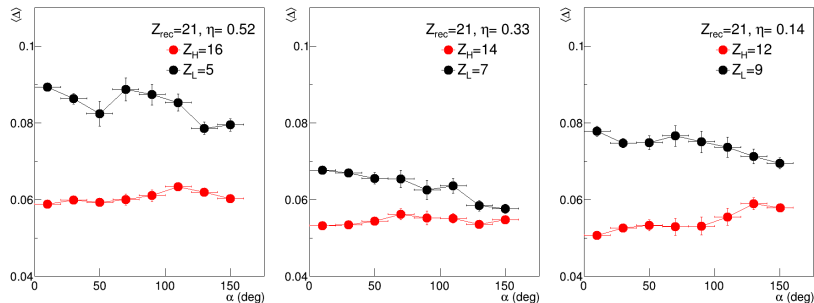
from A. Jedye et al., PRL118, 062501 (2017)

- However, no correlation between the α angle and $(t_{\text{breakup}} - t_{\text{QP-QT}})$ has been found in the framework of AMD

from S. Piantelli et al., PRC101, 034613 (2020)

Characteristics of the breakup fragments

Isospin equilibration between HF and LF

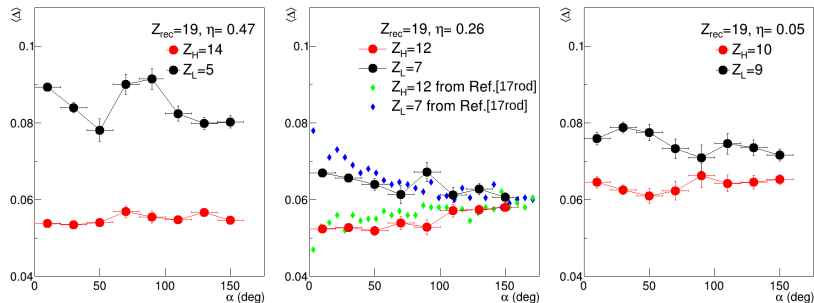


$\langle \Delta \rangle = \langle \frac{N-Z}{A} \rangle$ of the two breakup fragments as a function of the α angle:

- Data trends compatible with the picture proposed in literature:
 - LF more neutron rich than the HF.
 - larger HF-LF asymmetry for low α angles, more equilibrated for increasing α

Characteristics of the breakup fragments

Isospin equilibration between HF and LF



$\langle \Delta \rangle = \langle \frac{N-Z}{A} \rangle$ of the two breakup fragments as a function of the α angle:

- Data trends compatible with the picture proposed in literature:
 - LF more neutron rich than the HF.
 - larger HF-LF asymmetry for low α angles, more equilibrated for increasing α
- Within the small charge asymmetries explored, $\langle \Delta \rangle_L$ depends mostly on the identity of the LF, and less on the partner HF
- Results for $Z_H = 12, Z_L = 7$ are quite comparable to [A. Rodriguez Manso et al., PRC95, 044604 \(2017\)](#)